SPE 168622

Limited Height Growth and Reduced Opening of Hydraulic Fractures due to Fracture Offsets: An XFEM Application

Safdar Abbas, Schlumberger, Elizaveta Gordeliy and Anthony Peirce, University of British Columbia, Brice Lecampion, Dimitry Chuprakov and Romain Prioul, Schlumberger

This paper was prepared for presentation at the SPE Hydraulic Fracturing Technology Conference held in The Woodlands, Texas, USA, 4–6 February 2014.

Abstract

Hydraulic fracture propagation through a layered medium often exhibits a complex fracture path due to lateral shifting of the fracture path after passing through an interface. The existence of these offsets in the fracture path has been confirmed by mapping of mined fractures and by laboratory experiments. In addition to the stress contrast and material contrast, these offsets act as another mechanism for fracture-height containment. In order to investigate fracture height growth problem, we have considered a case of plane-strain fractures propagating from an injection point and propagating in a predetermined path. Fracture offsets of a given length and angle are prescribed within the predetermined path. In this way, we parametrize the problem of fracture offsets in order to quantify their effects on the fracture height growth and fracture opening reduction at the fracture offset (pinching effect). This is done while keeping a hydrostatic state of confining stresses in order to observe only the geometric effect of the fracture offset. We use a recently developed hydraulic fracturing code based on the eXtended Finite Element Method (XFEM). This code solves the fluid flow in the fracture and the elastic response of the fracture in a fully coupled manner solving for the fracture velocity using the complete hydraulic fracture tip asymptotics.

For different combinations of independent parameters (i.e., formation moduli, far-field stresses, fluid injection rate, ratio of offset length to the length of the straight fracture and the offset angles) we investigate the effect on the fracture height growth and the reduction in fracture opening at the fracture offset. A detailed parametric study shows that while each parameter affects the fracture height containment, the fracture opening reduction is dominated by the fracture offset angle which is a geometric effect of the fracture offsets. This has a profound effect on the proppant bridging at the fracture offset.

Introduction

Hydraulic fracture treatments are designed in order to restrict the fracture within the pay zone. If the fracture crosses into the adjacent rock formations, an excessive amount of material and effort is wasted in fracturing unproductive zone. In contrast, if the designed height of the hydraulic fractures is not achieved then a large area of the productive zone is not stimulated which affects the production rates. For this reason, numerical prediction of the fracture height growth has been an important field of research in hydraulic fracture modeling. Traditionally, fracture height growth has been associated with stress (Palmer and Carroll Jr. (1983); Jeffrey and Bunger (2009); Adachi et al. (2010)) and modulus contrast (Van Eekelen (1982); Gu and Siebrits (2008)) between adjacent layers. During a number of field studies it was found that the fracture height growth is less than that predicted by various numerical models considering modulus and stress contrast only. This led to the research in the fracture height containment due to weak mechanical interfaces (Van Eekelen (1982); Teufel and Clark (1984); Barree and Winterfeld (1998); Miskimins and Barree (2003); Athavale and Miskimins (2008)). When a hydraulic fracture interacts with a weak interface, either it crosses the interface, it is blunted and stopped at the interface or the hydraulic fracture develops a fracture offset (Beugelsdijk et al. (2000); Wu et al. (2004)).

There has been a number of studies which involve hydraulic fracturing before mining operations and then mining through the formation and observing the hydraulic fractures (Boyer II et al. (1986); Fisher and Warpinski (2012); Jeffrey et al. (2009)). One of the common features of hydraulic fractures found in all of these studies is the presence of fracture offsets. Many laboratory experiments have also verified these findings (Chudnovsky et al. (2001); Warpinski (1991); Hanson et al. (1981); Zhang and Jeffrey (2008); Zhang et al. (2007); Thiercelin et al. (1987)). There has been a number of studies which focused on the mechanism that leads to the development of these fracture offsets. These offsets develop as a result of the interaction between a propagating hydraulic fracture and the bedding planes which act as the planes of weakness. Different models were developed as the result of these studies which explained the factors affecting fracture crossing, arresting or offsetting. Stress contrast, angle and interface friction have been identified as the parameters affecting the result of this interaction. In a recent development, fluid injection rate/viscosity has been identified, experimentally by Beugelsdijk et al. (2000), semi analytically by Chuprakov et al. (2013a,b); Kresse et al. (2013) and in a hydraulic fracture model by Kresse et al. (2013), as one of the important factors affecting the fracture outcome of such an interaction.

In this study, we are interested in finding out the effect of a fracture offset after it has been created. Once the fracture offset has been created, it affects the fracture height growth by slowing down fracture propagation in vertical direction. The fracture offset also acts as a restriction in the fluid flow path which causes an increase in the treating pressure. This reduced fracture opening also results in proppant bridging in the fracture offset. This may result in the loss of the stimulated area ahead of the fracture offset due to fracture closure after the fluid pumping is stopped at the end of the fracturing treatment. This investigation will quantify the effect of geometric parameters of a fracture offset namely its length and angle. These parameters affect the fracture height growth and reduce the fracture opening in the fracture offset as discussed by Jeffrey et al. (2009, a) and Jeffrey et al. (2009, b). In both of these studies, the opening at the fracture offsets is affected by the difference in the far field stresses which are higher in the direction of fracture propagation as compared to the direction of fracture opening. In this contribution, we have assumed that there is no difference in the vertical confining stress and the minimum horizontal principal stress thus eliminating any effect associated with the difference in confining stresses in the two directions. This is done in order to study the solely geometric effects of the fracture offsets. Using a recently developed numerical code based on the eXtended Finite Element Method (XFEM) (Gordeliy and Peirce (2013a,b)) a hydraulic fracture is propagated symmetrically through a prescribed path which includes fracture offsets at a given distance. This allows for the simulation of hydraulic fracture propagation taking into account the full fluid-solid coupling using the correct fracture tip velocity. In addition to the geometry of the fracture offsets we have also studied the effects of injection rate, material properties and the confining stresses on the fracture height growth and the reduction in the fracture opening at the fracture offset.

Numerical Scheme

The hydraulic fracture propagation is simulated using a recently developed numerical algorithm based on the eXtended Finite Element Method (XFEM). This algorithm relies on the XFEM to solve the elastic component of the coupled elasto-hydrodynamic equations. The XFEM has an advantage over the traditional finite element method in simulating fracture mechanics (Belytschko and Black (1999); Moës et al. (1999); Fries and Belytschko (2010)). The finite element mesh is not needed to conform to the fracture geometry which avoids any kind of mesh manipulation during the fracture propagation. In addition to that, the singular fields at the fracture tip are resolved by enriching the approximation space by using appropriate *enrichment functions* (Fries and Belytschko (2010)) thus avoiding mesh refinement at the fracture tip. For the hydrodynamic part of the coupled problem, the conservation of the viscous fluid flowing within the fracture is described by the Reynolds lubrication equation which represents a degenerate PDE. This equation is solved in a fully coupled manner with the equations of elastic equilibrium for a solid body in the state of plane strain. In order to avoid solving a degenerate PDE for the singular pressure at the fracture tip and in order to incorporate a tip asymptotic solution, applicable at the computational length scale, a mixed scheme is used. In this mixed scheme, the fracture is divided into two regions, i.e. a channel region and a tip region. The tip asymptotic solution is prescribed in the tip region as the displacement jump using the localized mixed hybrid formulation of Zilian and Fries (2009). For the channel region, the applied fluid pressure, obtained from the lubrication equation, serves as the boundary condition at the crack faces within the XFEM formulation. The resulting fracture opening in the channel is computed from the XFEM solution for the fracture with these mixed boundary conditions. . The dynamic fracture propagation involves locating the fracture tip for each time step which represents a free boundary in space. This free boundary is located by using the Implicit Level Set Algorithm (ILSA) (Peirce and Detournay (2008)). This algorithm is used in the context of the XFEM by Gordeliy and Peirce (2013b).

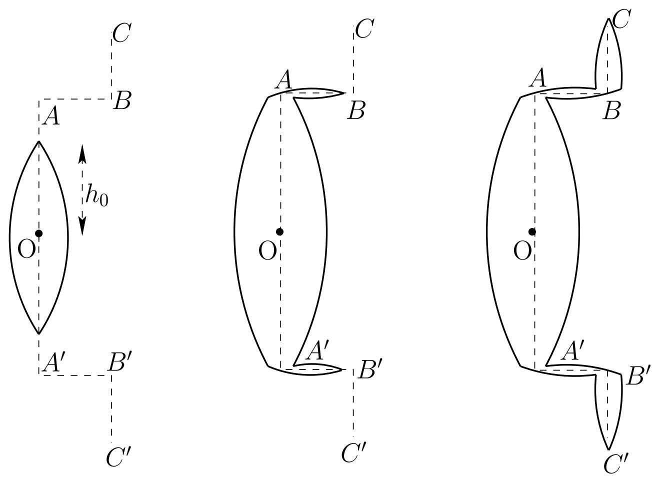

Fig. 1—Fracture propagation along a predetermined path.

In the current application we consider a hydraulic fracture growing in an impermeable elastic rock in a state of plane strain. The rock stiffness is characterized by the Young's modulus E and Poisson's ratio ν. The rock fracture toughness K_{Ic} characterizes the breaking strength of the rock. The fracture is assumed to be driven by a Newtonian fluid with a viscosity μ. The fluid is injected at a

Table 1—Material parameters for simulations.

	E (psi)	ν (-)	K (psi$\sqrt{\text{in}}$)	$\sigma_v = \sigma_h$ (psi)	E' (psi)	K' (psi$\sqrt{\text{in}}$)
Limestone	3.75×10^6	0.24	480	6474	3.99×10^6	1531.93
Shale	2.176×10^6	0.17	1500	6063	2.24×10^6	4787.3

constant volumetric injection rate Q_0 per unit length in the out-of-plane direction from a point source. The initial fracture geometry corresponds to a longitudinal fracture propagating from a horizontal wellbore with initial height h_0. The initial fracture opening and pressure corresponds to the analytical solution (Adachi and Detournay (2002)) of a symmetric plane strain hydraulic fracture for a given rock material parameters, fluid viscosity, constant injection rate and fracture half-length (initial height h_0, see Figure 1). As the fluid is injected with a constant rate, the pressure inside the fracture increases with time and the fracture starts to grow symmetrically along the path described by the dashed lines $OABC$ and $OA'B'C'$ in Figure 1.

Results and Discussion

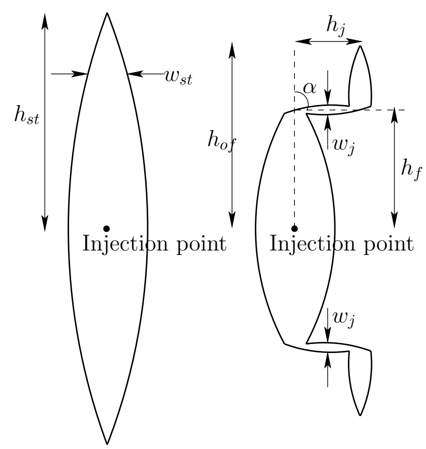

Fig. 2—Introduction of the opening and the length terms in the case of a straight fracture and a fracture with an offset.

Table 2—Parameter space for simulations.

Q bpm	$\frac{h_j}{h_f}$ (-)	h_f (ft)	h_j (ft)	h_0 (ft)	α (-)
$[1,40]$	$[0.01, 0.04]$	$[95,25]$	$[1,1]$	$[31.5,22.5]$	$[60,70,80,90]$

In order to compare the test cases with different fluid injection rates in different rock materials the dimensionless toughness $\mathcal{K}$ is computed for each case. The dimensionless toughness $\mathcal{K}$ for plane strain hydraulic fracture geometry propagating in an elastic impermeable medium is expressed as (Detournay (2004)):

$$\mathcal{K} = \frac{K'}{(\mu' E'^3 Q_0)^{1/4}}, \qquad (1)$$

where μ' is dynamic viscosity given as $\mu' = 12\mu$. The dimensionless toughness less than 3 indicates that the fracture is propagating in the viscosity dominated regime which means that there is a large fluid pressure drop inside the fracture and more energy is used to push the fluid in the fracture than it is needed to fracture the rock. We have run a number of simulations using the XFEM code for the hydraulic fracture propagation through a prescribed path. The fracture is assumed to have a propagation path with offsets of a given length and angle. It is assumed that the vertical stress is equal to the minimum principal stress and that there is no material or stress contrast across the fracture offset. In this way only the geometric effect of the fracture offsets is considered. All the test cases considered are symmetrical where two longitudinal fractures are initiated from the top and the bottom of a horizontal wellbore. These fractures propagate and encounter fracture offsets of a given size h_j and angle α at a given fracture length h_f as shown in Figure 2. In the test cases, limestone is considered as an example of a harder rock and shale is considered as an example of a softer rock. Material properties and the confining stresses for each rock type are based on the real data from Eagleford shale (1). Water is considered as the fracturing fluid in all the test cases with the viscosity of 1 cP. The fluid is pumped at two different rates in order to see the effect

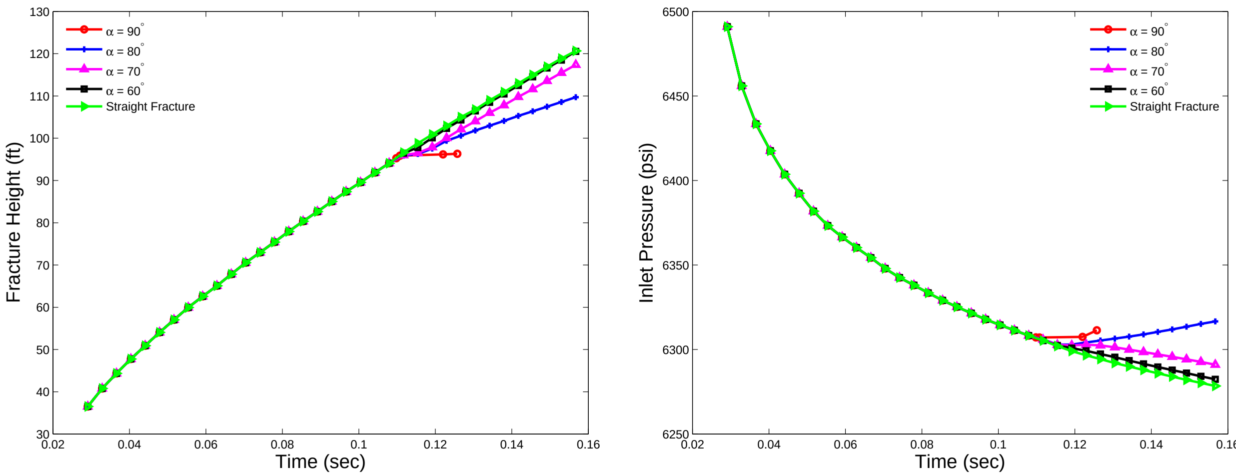

Fig. 3—The effect of fracture offset angle on the fracture height and inlet pressure for Shale with $Q = 4$ bpm, $\frac{h_j}{h_f} = 0.01$ ft, $h_f = 95$ ft, $h_0 = 31.5$ ft.

of high and low injection rates on the fracture height growth. Two cases of fracture offset condition are considered. One with the short offset as compared to the fracture length, i.e. smaller ratio h_j/h_f, and the other with a longer offset as compared to the fracture length, i.e. larger ratio h_j/h_f, see 2. In all the test cases, the time delay and the reduction in fracture opening at the middle of the fracture offset (i.e., at $h_j/2$) are evaluated for several values of fracture offset angle α given in 2.

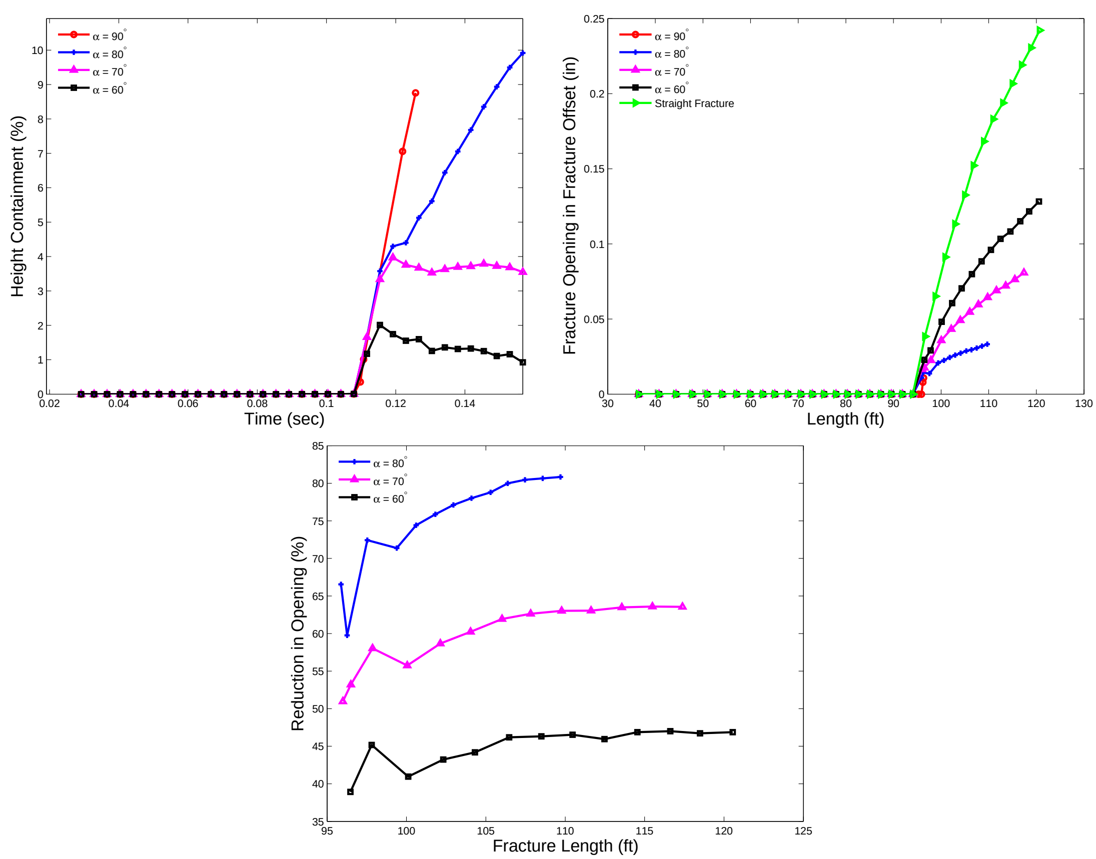

Fig. 4—Height containment and opening reduction for Shale with $Q = 40$ bpm, $\mathcal{K} = 0.2538$ small-offset $\left(\frac{h_j}{h_f} = 0.01 \text{ ft}, h_f = 95 \text{ ft}, h_0 = 31.5 \text{ ft}\right)$.

The effect of the angle of the fracture offset on the fracture height growth can be seen from Figure 3 (left). This is the case of

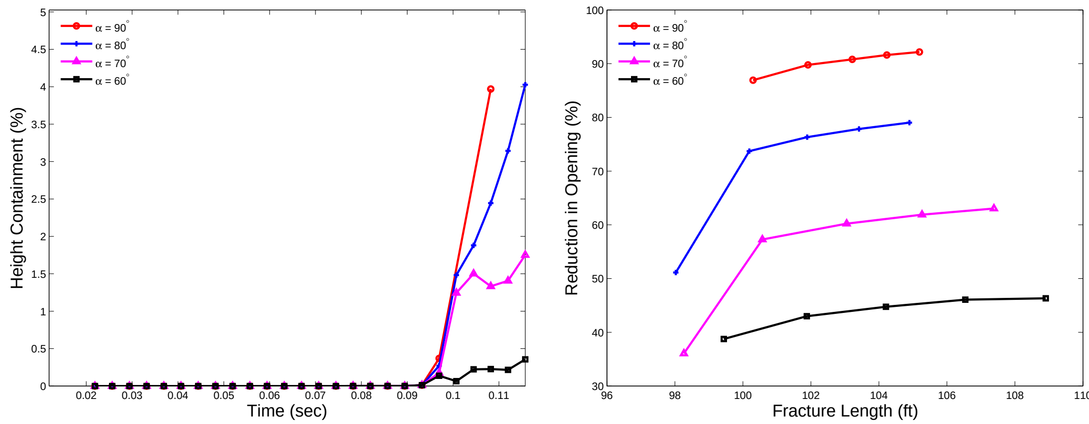

Fig. 5—Height containment and opening reduction for Limestone with $Q = 40$ **bpm**, $\mathcal{K} = 0.0527$ small-offset $\left(\frac{h_j}{h_f} = 0.01 \text{ ft}, h_f = 95 \text{ ft}, h_0 = 31.5 \text{ ft}\right)$.

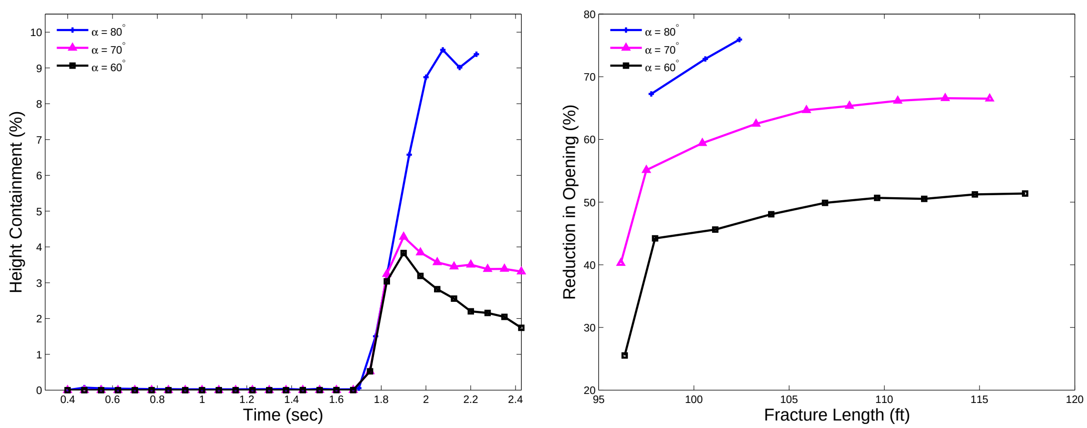

Fig. 6—Height containment and opening reduction for Shale with $Q = 1$ **bpm**, $\mathcal{K} = 0.6384$ small-offset $\left(\frac{h_j}{h_f} = 0.01 \text{ ft}, h_f = 95 \text{ ft}, h_0 = 31.5 \text{ ft}\right)$.

a fracture propagating in the shale formation (lower confining stress) with the high fluid injection rate $Q = 40$ bpm. Length of the fracture before the fracture offset is $h_f = 95$. In the case of 90° fracture offset, the fracture slows down as it reaches the fracture offset and stops just after crossing the offset. In the case of 80° and 70° offset angles, fracture propagation velocity is considerably reduced but the fracture is not stopped. The fracture inlet pressure at the wellbore is plotted against time for this case in Figure 3 (right). This plot reveals that a significant increase in the wellbore pressure is observed in the case of 90°, 80° and 70° fracture angles. This pressure increase at the fracture inlet can be considered as one of the diagnostic features of the situation when a fracture encounters a fracture offset in the propagation path.

Next we look at the effect of fracture offsets on fracture height growth. The fracture height containment is computed using the fracture height versus time plot in Figure 3 (left). The height containment is defined as the percentage reduction in fracture height at a given time in fracture propagation (see Figure 2).

$$\% \text{ Height Containment} = \frac{h_{st} - h_{of}}{h_{st}} \times 100, \quad \text{(2)}$$

where h_{st} is the height of the fracture with no fracture offset at the same time when the height of the offset fracture is h_{of}. The reduction in fracture height growth with time for the previous case is plotted for each fracture offset angle in Figure 4 (top-left). It is obvious from this plot that the fracture offsets affect the fracture height growth depending upon the offset angle. Higher the offset angle, higher is the fracture height containment in this case. As soon as the fracture reaches the fracture offset, it starts to lose fracture height. The fracture height containment becomes nearly constant after achieving a maximum value. The same characteristic behavior is observed for all the test cases considered, see Figures 5 to 11 (left figures). In most of the test cases, the fracture with the 90° offset was not able to propagate through the fracture offset. Only in the case of the limestone, with high rate of flow and smaller ratio h_j/h_f, the fracture with 90° offset propagated through the offset, see Figure 5 (left). In the test case for shale with $Q = 1$ bpm and large ratio h_j/h_f, the fracture with 80° offset was also not able to propagate through the fracture offset, see Figure 10 (left).

Another effect of the fracture offsets is that the energy used to open the main fracture is consumed in shearing the fracture offset.

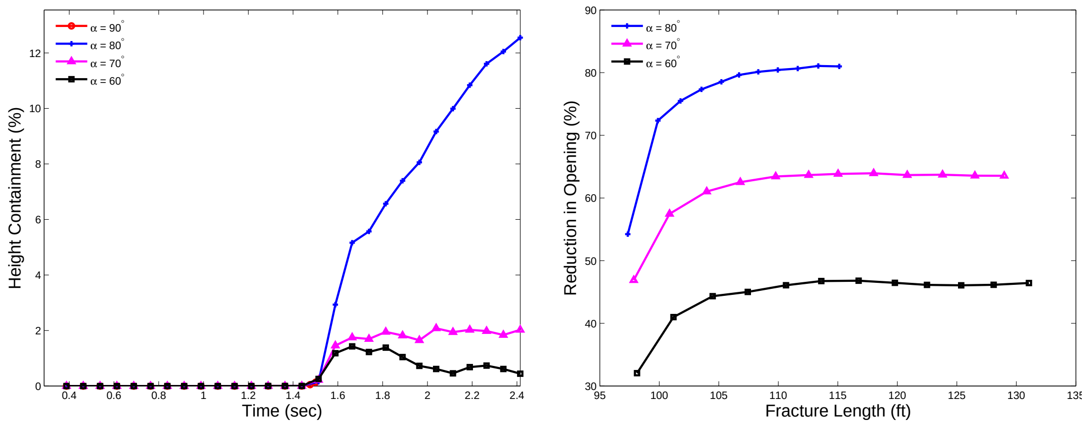

Fig. 7—Height containment and opening reduction for Limestone with $Q = 1$ **bpm,** $\mathcal{K} = 0.1325$ **small-offset** $\left(\frac{h_j}{h_f} = 0.01 \textbf{ ft}, h_f = 95 \textbf{ ft}, h_0 = 31.5 \textbf{ ft}\right)$**.**

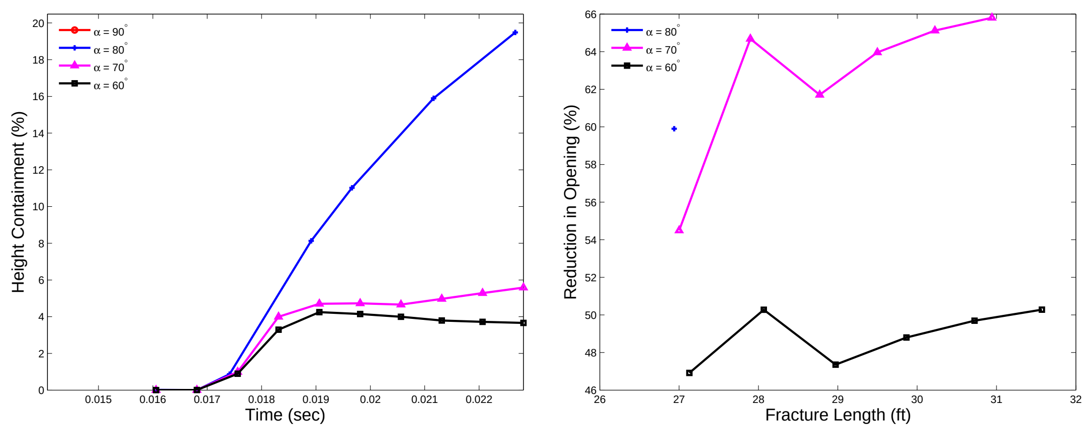

Fig. 8—Height containment and opening reduction for Shale with $Q = 40$ **bpm,** $\mathcal{K} = 0.2538$ ***Large-offset*** $\left(\frac{h_j}{h_f} = 0.04 \textbf{ ft}, h_f = 25 \textbf{ ft}, h_0 = 22.5 \textbf{ ft}\right)$**.**

This causes a fracture opening reduction (or pinching) at the fracture offset. This is defined as the percentage difference in the opening at the fracture offset as compared to the straight fracture (see Figure 2).

$$\% \text{ Width Reduction} = \frac{w_{st} - w_j}{w_{st}} \times 100, \quad (3)$$

where w_j is measured at the middle of the fracture offset i.e. at offset distance $h_j/2$ and w_{st} is measured at a distance of $h_f + h_j/2$ from the injection point. For the case of shale with $Q = 40$ bpm and small ratio h_j/h_f, the percentage reduction in fracture opening at the fracture offset is plotted in Figure 4 (right). The fracture opening is considerably reduced at the fracture offset. As soon as the fracture enters the fracture offset, the fracture opening in the offset decreases very quickly, see Figure 4 (right). After the fracture has propagated ahead of the fracture offset, the fracture opening keeps increasing in the fracture offset with nearly constant rate. Thus the percentage opening reduction in the fracture offset remains constant. It is worthwhile to remind the reader that in all the test cases we have considered a hydrostatic state of confining stresses, i.e. $\sigma_v = \sigma_h$. If we consider a deviatoric state of confining stresses with $\sigma_v > \sigma_h$, the rate of increase in fracture opening at the offset will be even lower. It can be observed in all the test cases that there is a huge influence of fracture offset angle on the fracture opening reduction at the fracture offset. Generally, there is a 10 to 15 percent reduction in fracture opening for each 10° increase in fracture offset angle α. There is no plot of fracture opening reduction for the larger offset angles in some cases. This is due to the fact that the fracture was not able to propagate through the fracture offset in those cases.

Next we investigate the parameter space given in Tables 1 and 2 to find out the effect of each parameter on fracture height growth and the fracture opening reduction. Each investigation covers all the fracture offset angles. In Figures 4 to 11 the fracture height containment is given as a function of time (figures on the left side) and the opening reduction as a function of fracture length (figures on the right side). For the sake of comparison the fracture height containment is considered at the time where the difference between the values is maximum for different offset angles. For example, the fracture height containment for the case in Figure 4 is computed at the time 0.1267 sec. Similarly, the opening reduction is considered at the fracture length where the difference between the values

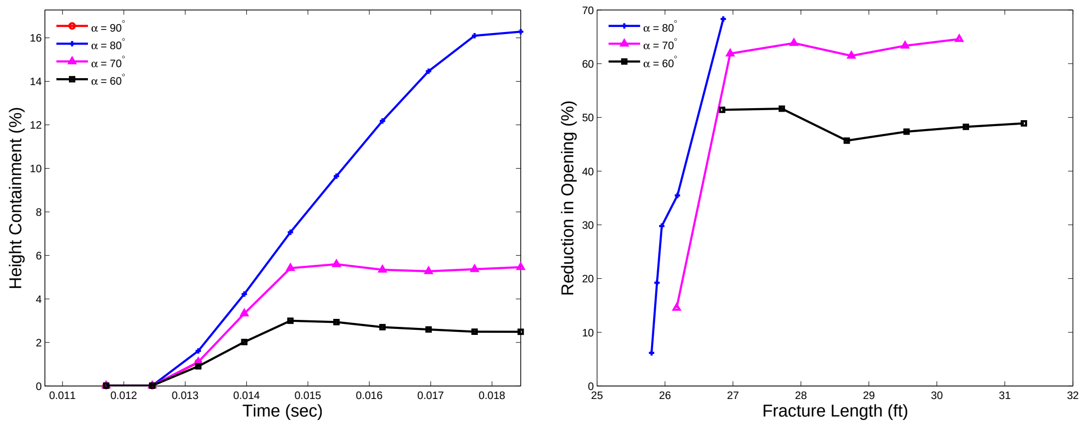

Fig. 9—Height containment and opening reduction for Limestone with $Q = 40$ bpm, $\mathcal{K} = 0.0527$ *Large-offset* $\left(\dfrac{h_j}{h_f} = 0.04 \text{ ft}, h_f = 25 \text{ ft}, h_0 = 22.5 \text{ ft}\right)$**.**

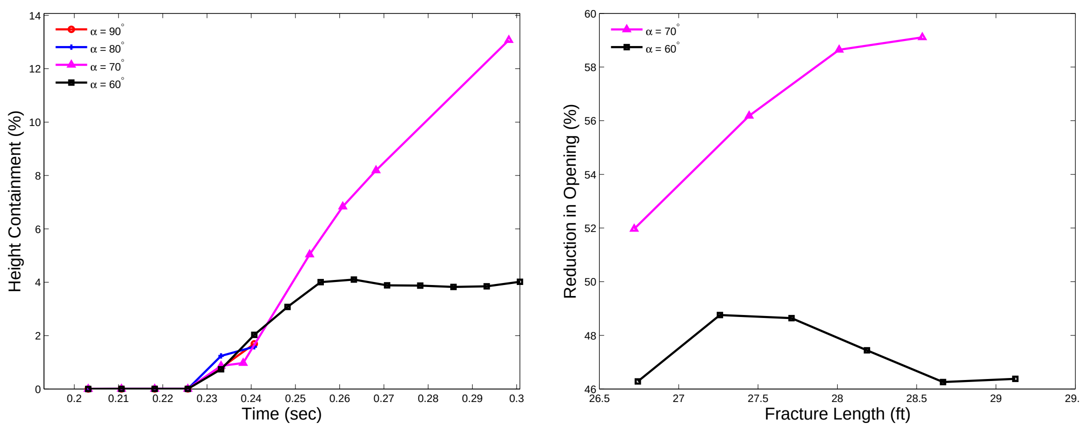

Fig. 10—Height containment and opening reduction for Shale with $Q = 1$ bpm, $\mathcal{K} = 0.6384$ *Large-offset* $\left(\dfrac{h_j}{h_f} = 0.04 \text{ ft}, h_f = 25 \text{ ft}, h_0 = 22.5 \text{ ft}\right)$**.**

is maximum for different offset angles. For example, fracture offset width reduction for the case in Figure 4 is computed at the fracture length of 109.7 ft. As the properties and the confining stresses are based on the real data, there is a change in the confining stresses with the material properties and vice versa. This makes it difficult to distinguish between the effect of material parameters and the confining stresses on the fracture height containment and the fracture opening reduction. In order to quantify these effects, we have carried out two investigations by manipulating the material properties and the corresponding confining stresses. All the other parameters i.e. $Q = 40$ bpm, $h_j/h_f = 0.04$ ft, $h_f = 25$ ft, $h_0 = 22.5$ ft are kept the same in these investigations. In the first investigation, the hydraulic fracture is propagated through the offsets of different offset angles for two two different materials: a) shale and b) limestone. The confining stresses are kept in a hydrostatic state with the magnitude equal to 6474 psi. The results in Figure 12 (left) show that there is more height containment for the material with larger moduli. In contrast to that there is not a large influence of the material parameters on the fracture opening reduction, see Figure 12 (right). In the case of 80° offset angle, fracture was not able to propagate through the 80° offset.

In the second investigation, the hydraulic fracture is propagated through the offsets of different offset angles for two different cases of confining stresses: a) lower confining stress of 6063 psi and b) higher confining stress of 6474 psi. In each case the confining stresses are kept in a hydrostatic state of stress. The rock material is kept as the limestone for both cases. It is obvious from the results in Figure 13 that there is more height containment for the higher confining stresses. In contrast to that there is not a large influence of the confining stresses on the fracture opening reduction. This behavior is very much similar to the effect of material parameters.

Now we investigate the effect of each parameter in Table 2 separately. Let us first consider the effect of fluid injection rate on the fracture height growth and the fracture opening reduction for the case of large fracture offset i.e. $h_j/h_f = 0.04$ ft, $h_f = 25$ ft, $h_0 = 22.5$ ft. It can be seen in Figure 14 (left) that there is more height containment in the case of low flow rate as compared to the high flow rate. The difference is more pronounced in the case of shale as compared to the case of limestone. The fractures with 90° offset angle and the fracture in shale with the 80° offset angle in the case of low rate of pumping were not able to propagate through the fracture offset so their results cannot be compared. The fracture opening reduction can be seen in Figure 14 (right). There is no clear trend in the fracture opening reduction when the high rate of injection is compared with the low rate of injection. The difference

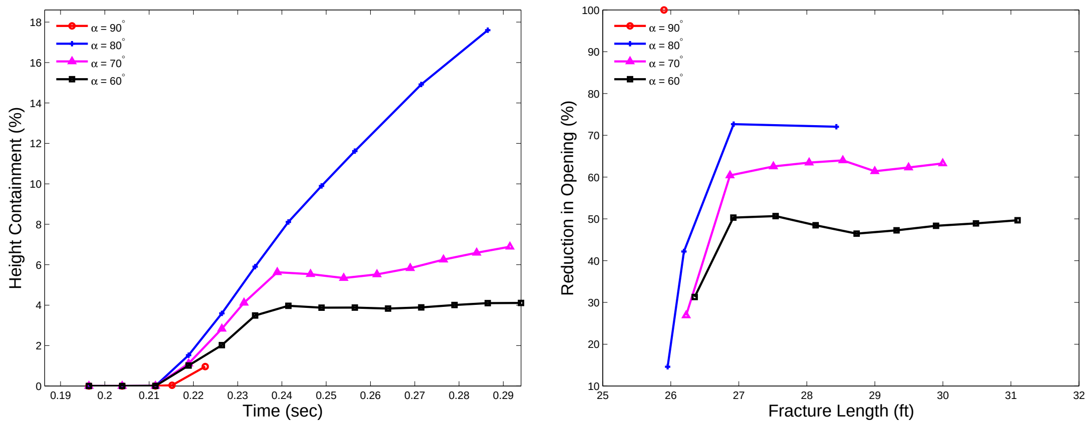

Fig. 11—Height containment and opening reduction for Limestone with $Q = 1$ bpm, $\mathcal{K} = 0.1325$ *Large-offset* $\left(\frac{h_j}{h_f} = 0.04\ \mathbf{ft}, h_f = 25\ \mathbf{ft}, h_0 = 22.5\ \mathbf{ft}\right)$**.**

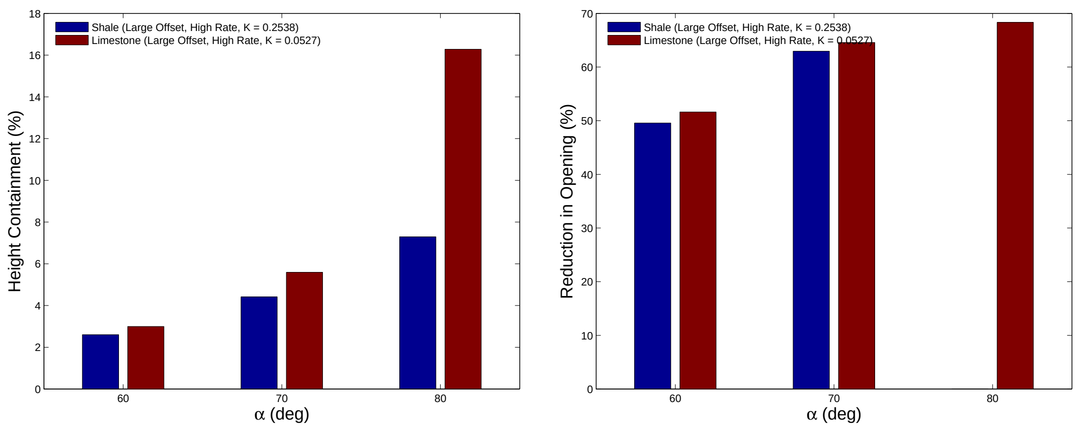

Fig. 12—Comparing the rock material for the same confining stress $\sigma_v = \sigma_h = 6474$ **psi**, $Q = 40$ **bpm**, $\frac{h_j}{h_f} = 0.04$ **ft**, $h_f = 25$ **ft**, $h_0 = 22.5$ **ft.**

in opening reduction for each material is within 2 to 5 percent range for each offset angle. In the case of small fracture offset in Figure 15 (right), same trends can be seen. There seems to be no effect of the pumping rate on the reduction in fracture offset opening. In the case of limestone with the low injection rate, there is relatively more height containment as compared to the same material and the higher injection rate.

The dimensionless fracture toughness $\mathcal{K}$ for all the test cases considered thus far is less than 3. This indicates the fracture propagation in the viscosity dominated regime. Let us also investigate the cases where the fracture propagation is dominated by the rock fracture toughness, i.e. the case of slow pressurization. In Figure 16 (right), it can be seen that, in the case of slow pressurization, the fracture velocity decreases considerably at the fracture offset. There is a sudden peak in height containment due to this reduction in fracture velocity, see Figure 17 (left). Once the fracture passes through the fracture offset the fracture velocity increases which results in a decrease in fracture height containment. There is no clear trend in the fracture opening reduction, see Figure 17 (right) but the fracture opening is reduced by 44 to 54 percent in both the cases of slow and fast pressurization. The injection rate for the toughness dominated propagation is so low that it is not practicle to have this injection rate during the hydraulic fracture stimulation. Even for this practically very low injection rate, the conclusion remains the same i.e., there is more height containment in the case of low flow rate as compared to the high flow rate. There is no clear trend in the fracture opening reduction when the high rate of injection is compared with the low rate of injection.

Let us now investigate the effect of the ratio h_j/h_f on fracture height growth and the pinching effect at the fracture offset. There is a clear trend which can be seen in Figures 18 and 19 which indicates that there is more height containment in the case of large fracture offsets as compared to the small fracture offsets. In terms of the pinching effect at the fracture offset, it seems that the pinching effect is more pronounced in the small offsets as compared to the large offsets with the exception of 60° offset angle. But even in that case the difference in the pinching effect at the fracture offset for small and the large offset is less than 5 percent. The trend is more obvious for larger fracture offset angles that the pinching effect is more dominant in the case of smaller fracture offsets as compared to the larger fracture offsets.

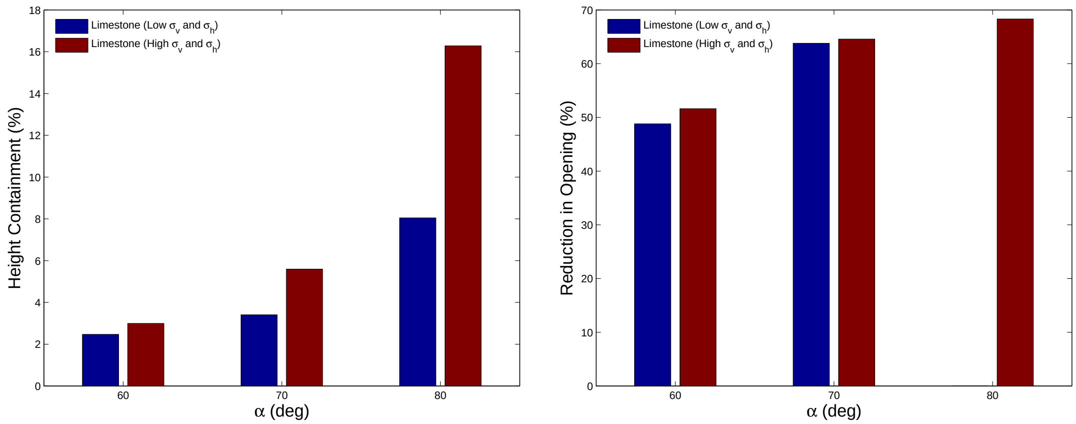

Fig. 13—Comparing the confining stress for the Limestone $Q = 40$ bpm, $\mathcal{K} = 0.0527$, $\frac{h_j}{h_f} = 0.04$ ft, $h_f = 25$ ft, $h_0 = 22.5$ ft.

The effect of injection rate Q in the case of toughness dominated fracture propagation

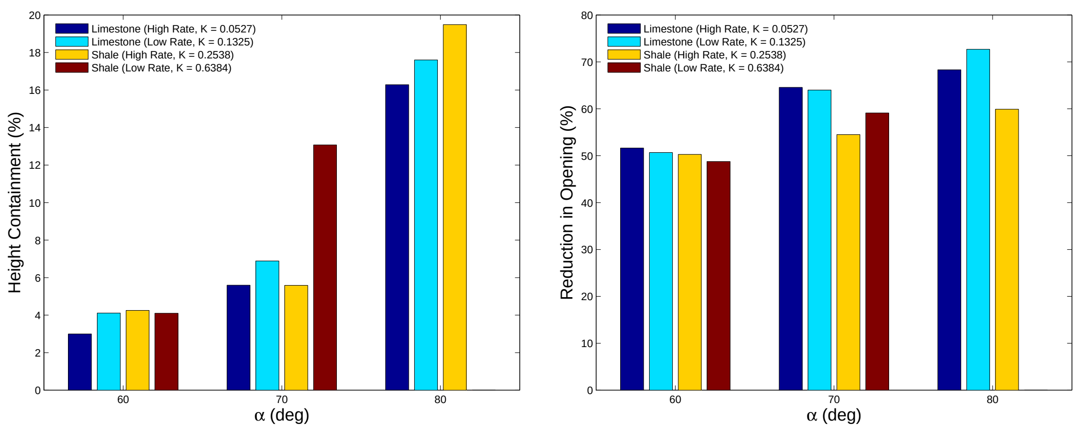

Fig. 14—The effect of injection rate Q in the case of large offset $\frac{h_j}{h_f} = 0.04$ ft, $h_f = 25$ ft, $h_0 = 22.5$ ft.

Conclusions

In this contribution we have applied a newly developed hydraulic fracture simulation code based on the eXtended Finite Element Method (XFEM) to a practical problem of hydraulic fracture propagation through fracture offsets of given length and angles. We have carried out a detailed parametric study of the problem of fracture offsets in order to evaluate the effect of each parameter on the fracture height growth and fracture opening reduction at the fracture offset. The geometric parameters of the problem include fracture offset angle,and the ratio of the fracture offset length to the length of the straight fracture. In addition to the geometric parameters, the effects of different material parameters, confining stresses and the fluid injection rate are considered. Among all the parameters considered, it was observed that the fracture offset angle has the most profound effect on fracture height growth and fracture opening reduction at the fracture offset. The same dependence of opening reduction on the offset angle was observed by Jeffrey et al. (2009, a) and Jeffrey et al. (2009, b) but the authors have attributed that to the difference in the confining stress normal to the main fracture and the fracture offset. In this contribution we have kept a hydrostatic state of confining stresses, in spite of that we have observed a strong dependence of height containment and fracture opening on the offset angle. This result shows that this dependence on the offset angle is actually an effect of the considered geometry which will be magnified in the case of confining stresses with a deviatoric component.

The results of the parametric study can be summarized as follows:

1. **Height containment:**
   - Higher offset angle α results in more height containment.
   - Larger material modulus results in more height containment.
   - Higher confining stress results in more height containment (for the considered injection parameters).
   - Lower injection rate results in more height containment. This is valid for the toughness dominated propagation as well as for the propagation in the viscosity dominated regime.

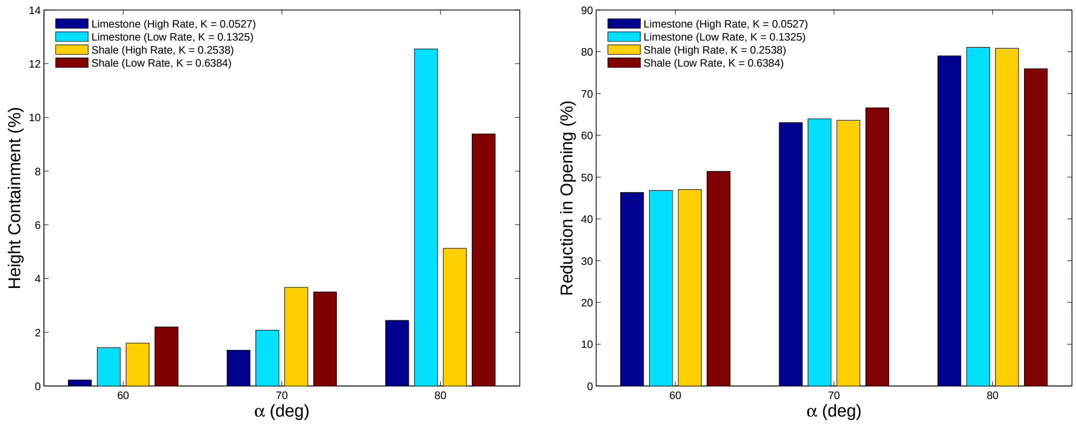

Fig. 15—The effect of injection rate Q in the case of small offset $\dfrac{h_j}{h_f} = 0.01$ **ft**, $h_f = 95$ **ft**, $h_0 = 31.5$ **ft.**

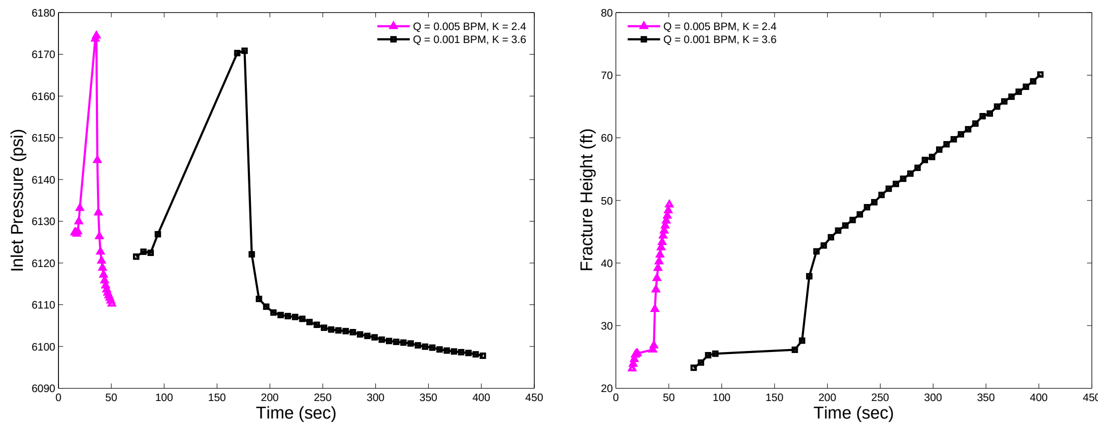

Fig. 16—Pressure response and fracture height growth in the case of slow pressurization $\alpha = 60°$, $\dfrac{h_j}{h_f} = 0.04$ **ft**, $h_f = 25$ **ft**, $h_0 = 22.5$ **ft.**

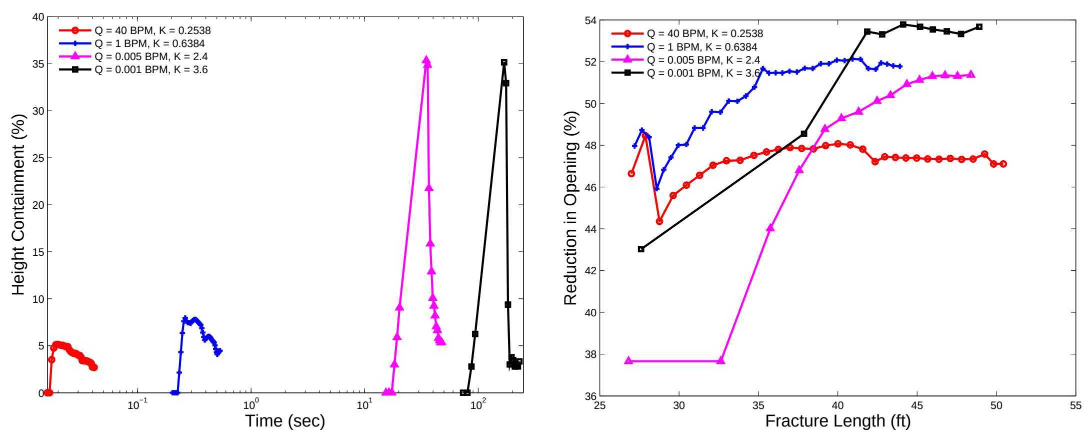

Fig. 17—The effect of injection rate Q in the case of toughness dominated fracture propagation $\alpha = 60°$, $\dfrac{h_j}{h_f} = 0.04$ **ft**, $h_f = 25$ **ft**, $h_0 = 22.5$ **ft.**

- Higher ratio of $\dfrac{h_j}{h_f}$ results in more height containment.

2. **Reduction in fracture opening:**

- Higher offset angle α results in more reduction in fracture opening at the fracture offset.

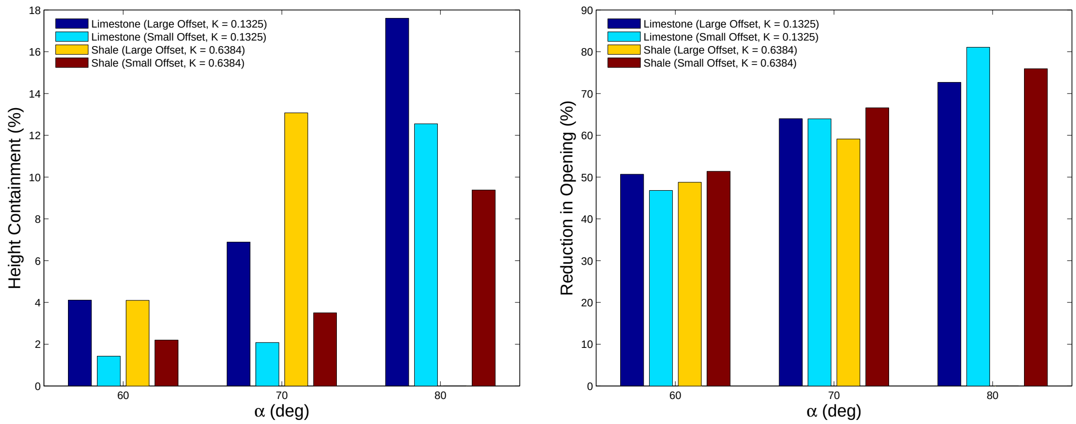

Fig. 18—The effect of fracture offset ratio $\frac{h_j}{h_f}$ in the case of low injection rate $Q = 1$ bpm.

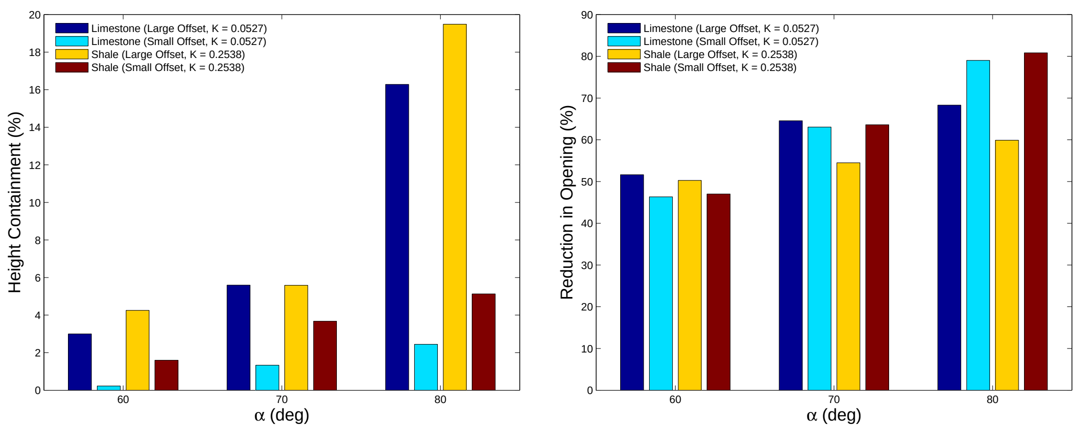

Fig. 19—The effect of fracture offset ratio $\frac{h_j}{h_f}$ in the case of high injection rate $Q = 40$ bpm.

- There is not an appreciable effect of material moduli on reduction in fracture opening at the fracture offset.
- There is not an appreciable effect of confining stress on reduction in fracture opening at the fracture offset.
- There is not an appreciable effect of injection rate on reduction in fracture opening at the fracture offset. The fracture opening is reduced by 45 to 55 percent for the toughness dominated propagation as well as for the viscosity dominated propagation.
- Generally, lower ratio of $\frac{h_j}{h_f}$ results in more reduction in fracture opening. For small offset angles, higher ratio of $\frac{h_j}{h_f}$ results in more reduction in fracture opening.

This study concludes that while each parameter affects the fracture height containment, the fracture opening reduction is dominated by the fracture offset angle which is a geometric effect of the fracture offsets. These fracture offsets generally develop at the weak interfaces between the bed boundaries. In this study we have not considered the effect of deviatoric confining stresses and the frictional interfaces. In the absence of frictional interfaces all the energy used to open the main fracture is consumed to shear the fracture offset. In reality, some of the energy used to open the main fracture is dissipated at the frictional interface. Some of the fluid will also leak into the weak interfaces, this eventually further reduces the fracture opening at the fracture offset. In this way, this study shows the lower bound in terms of the fracture height containment and opening reduction due to fracture offsets. Any consideration of the confining stresses with a deviatoric component and frictional interface is going to magnify this effect.

References

Adachi, J. and E. Detournay (2002). Self-similar solution of a plane-strain fracture driven by a power-law fluid. *International Journal for Numerical and Analytical Methods in Geomechanics 26*(6), 579–604.

Adachi, J. I., E. Detournay, and A. P. Peirce (2010). Analysis of the classical pseudo-3d model for hydraulic fracture with equilibrium height growth across stress barriers. *International Journal of Rock Mechanics and Mining Sciences 47*(4), 625–639.

Athavale, A. and J. Miskimins (2008). Laboratory hydraulic fracturing tests on small homogeneous and laminated blocks. In *The 42nd U.S. Rock Mechanics Symposium (USRMS), June 29 - July 2, 2008 , San Francisco, CA*, Number 08-067. American Rock Mechanics Association.

Barree, R. and P. Winterfeld (1998). Effects of shear planes and interfacial slippage on fracture growth and treating pressures. In *SPE Annual Technical Conference and Exhibition, 27-30 September 1998, New Orleans, Louisiana*, Number 48926. Society of Petroleum Engineers.

Belytschko, T. and T. Black (1999). Elastic crack growth in finite elements with minimal remeshing. *Internat. J. Numer. Methods Engrg. 45*, 601 – 620.

Beugelsdijk, L., C. dePater, and K. Sato (2000). Experimental hydraulic fracture propagation in a multi-fractured medium. In *SPE Asia Pacific Conference on Integrated Modelling for Asset Management, 25-26 April 2000, Yokohama, Japan*, Number 59419. Society of Petroleum Engineers.

Boyer II, C. M., P. Stubbs, and F. Scherer (1986). Measurement of coalbed properties for hydraulic fracture design and methane production. In *SPE Unconventional Gas Technology Symposium*, Number SPE 15258. Society of Petroleum Engineers. SPE Unconventional Gas Technology Symposium, 18-21 May 1986, Louisville, Kentucky.

Chudnovsky, A., J. Fan, Y. Shulkin, J. W. Dudley, W. B. Nichols, and G. K. Wong (2001). Hydraulic fracture containment in layered media, experiment and computer simulation. In *38th U.S. Symposium on Rock Mechanics (USRMS)*, Number ARMA 01-0273. American Rock Mechanics Association.

Chuprakov, D., O. Melchaeva, and R. Prioul (2013a). *Effective and Sustainable Hydraulic Fracturing*, Chapter 8: Hydraulic Fracture Propagation Across a Weak Discontinuity Controlled by Fluid Injection, pp. 157–182. InTech.

Chuprakov, D., O. Melchaeva, and R. Prioul (2013b). Injection-sensitive mechanics of hydraulic fracture interaction with discontinuities, ARMA 13-252. In *47th US Rock Mechanics Geomechanics Symposium*. American Rock Mechanics Association.

Detournay, E. (2004). Propagation regimes of fluid-driven fractures in impermeable rocks. *International Journal of Geomechanics 4*(1), 35–45.

Fisher, M. K. and N. R. Warpinski (2012). *SPE Production & Operations 27*(1), 8–19.

Fries, T. and T. Belytschko (2010). The extended/generalized finite element method: An overview of the method and its applications. *Internat. J. Numer. Methods Engrg. 84*, 253 – 304.

Gordeliy, E. and A. Peirce (2013a). Coupling schemes for modeling hydraulic fracture propagation using the XFEM . *Computer Methods in Applied Mechanics and Engineering 253*(0), 305 – 322.

Gordeliy, E. and A. Peirce (2013b). Implicit level set schemes for modeling hydraulic fractures using the XFEM. *Computer Methods in Applied Mechanics and Engineering 266*(0), 125 – 143.

Gu, H. and E. Siebrits (2008). Effect of formation modulus contrast on hydraulic fracture height containment. *SPE Production & Operations 23*(2), 170–176.

Hanson, M. E., R. J. Shaffer, and G. D. Anderson (1981). Effects of various parameters on hydraulic fracturing geometry. *SPE Journal 21*(4), 435–443.

Jeffrey, R. and A. Bunger (2009). A detailed comparison of experimental and numerical data on hydraulic fracture height growth through stress contrasts. *SPE Journal 14*(3), 413–422.

Jeffrey, R., A. Bunger, B. Lecampion, X. Zhang, Z. Chen, A. van As, D. Allison, W. De Beer, J. Dudley, E. Siebrits, et al. (2009). Measuring Hydraulic Fracture Growth in Naturally Fractured Rock. In *SPE Annual Technical Conference and Exhibition*, pp. SPE 124919.

Jeffrey, R., A. Bunger, B. Lecampion, X. Zhang, Z. Chen, A. van As, D. Allison, W. de Beer, J. Dudley, E. Siebrits, M. Thiercelin, and M. Mainguy (2009). Measuring hydraulic fracture growth in naturally fractured rock. In *SPE Annual Technical Conference*, Number SPE 124919. Society of Petroleum Engineers.

Jeffrey, R., X. Zhang, and M. Thiercelin (2009). Hydraulic fracture offsetting in naturally fractured reservoirs: Quantifying a long-recognized process. In *SPE Hydraulic Fracturing Technology Conference*, Number SPE 119351. Society of Petroleum Engineers.

Kresse, O., X. Weng, D. Chuprakov, R. Prioul, and C. Cohen (2013). *Effective and Sustainable Hydraulic Fracturing*, Chapter 9: Effect of Flow Rate and Viscosity on Complex Fracture Development in UFM Model, pp. 183–210. InTech.

Miskimins, J. L. and R. D. Barree (2003). Modeling of hydraulic fracture height containment in laminated sand and shale sequences. In *SPE Production and Operations Symposium, 22-25 March 2003, Oklahoma City, Oklahoma*, Number 80935. Society of Petroleum Engineers.

Moës, N., J. Dolbow, and T. Belytschko (1999). A finite element method for crack growth without remeshing. *Internat. J. Numer. Methods Engrg. 46*, 131 – 150.

Palmer, I. D. and H. Carroll Jr. (1983). Three-dimensional hydraulic fracture propagation in the presence of stress variations. *SPE Journal 23*(6), 870–878.

Peirce, A. P. and E. Detournay (2008, June). An implicit level set method for modeling hydraulically driven fractures. *Computer Methods in Applied Mechanics and Engineering 197*(33-40), 2858–2885.

Teufel, L. W. and J. A. Clark (1984). Hydraulic fracture propagation in layered rock: Experimental studies of fracture containment. *SPE Journal 24*(1), 19–32.

Thiercelin, M., J. Roegiers, T. Boone, and A. Ingraffea (1987). An investigation of the material parameters that govern the behavior of fractures approaching rock interfaces. In *6th ISRM Congress, August 30 - September 3, 1987 , Montreal, Canada*, Number 6CONGRESS-1987-049. International Society for Rock Mechanics.

Van Eekelen, H. (1982). Hydraulic fracture geometry: Fracture containment in layered formations. *SPE Journal 22*(3), 341–349.

Warpinski, N. R. (1991). Hydraulic fracturing in tight, fissured media. *Journal of Petroleum Technology 43*(2), 146–151, 208–209.

Wu, H., A. Chudnovsky, J. Dudley, and G. Wong (2004). A map of fracture behavior in the vicinity of an interface. In *Gulf Rocks 2004, the 6th North America Rock Mechanics Symposium (NARMS), June 5 - 9, 2004 , Houston, Texas*, Number 04-620. American Rock Mechanics Association.

Zhang, X. and R. G. Jeffrey (2008). Reinitiation or termination of fluid-driven fractures at frictional bedding interfaces. *Journal of Geophysical Research-Solid Earth 113*(B8).

Zhang, X., R. G. Jeffrey, and M. Thiercelin (2007). Deflection and propagation of fluid-driven fractures at frictional bedding interfaces: A numerical investigation. *Journal of Structural Geology 29*(3), 396–410.

Zilian, A. and T. Fries (2009). A localized mixed-hybrid method for imposing interfacial constraints in the extended finite element method (XFEM). *Internat. J. Numer. Methods Engrg.*, DOI: 10.1002/nme.2596.